FEATURE ARTICLE

Inelastic Neutron Scattering: A Tool in Molecular Vibrational Spectroscopy and a Test of ab Initio Methods

Bruce S. Hudson*

Department of Chemistry and W. M. Keck Center for Molecular Electronics, Syracuse University, Syracuse, New York 13244-4100

Received: December 7, 2000; In Final Form: February 14, 2001

Inelastic neutron scattering (INS) as discussed in this article is a technique for studies of the atomic vibrations of solids at low temperature. Unique features of this method are the absence of selection rules and the predominance of scattering due to the motion of hydrogen (but not deuterium) atoms. The scattering from hydrogen is given by a sum of intensities from individual atoms and is easily calculated from a normal mode treatment. When hydrogen is absent, the scattering is usually dominated by coherent contributions involving the motions of pairs of atoms. In either case, ab initio methods can be tested by comparison of the calculated INS spectral intensities as well as the frequencies of molecular vibrations with the observed spectra. For molecular solids, these spectra may be interpreted in molecular terms. In cases where intermolecular interactions are important, these must be included explicitly. Hydrogen-bonded systems are of greatest interest in this respect. Selective deuteration of hydrogen-bonded systems can be used to provide detailed tests of the potential surfaces. At some level of resolution, the effects of intermolecular interactions are revealed even for hydrocarbons.

Introduction

Inelastic neutron scattering as used for vibrational spectroscopy is very similar conceptually to Raman scattering. The quantity measured is the change in energy of the radiation, reflecting an excitation of the material under investigation. The major difference is that with neutrons the interaction is with the nuclei rather than with the electrons of the sample. This interaction depends on nuclear forces and is consequently very dependent on the specific nuclide in question. Most important in this respect is that the scattering by hydrogen is much stronger than that by deuterium (^{2}H) nuclei. In fact, scattering by hydrogen is considerably stronger than by any other nucleus and thus dominates the signal if present. For nuclei with spin, the interaction is different for the distinct relative orientations of the neutron and nuclear spins. If the nuclear and neutron spins are random in orientation, this results in "incoherent" scattering as discussed in more detail below. Incoherent scattering depends on the motion of individual atoms rather than pairs of atoms. This is the dominant scattering mechanism for hydrogen atoms. A comparison of scattering lengths, scattering cross sections, and absorption cross sections is given in Table 1.[1]

An important aspect of inelastic neutron scattering for neutrons with thermal energies is that the energy of the neutron is comparable to that of molecular vibrational excitations, and thus, the fractional energy change in an inelastic event is large. Thermal neutrons have de Broglie wavelengths that are on the order of a few angstroms. This leads to the use of such radiation for crystallographic diffraction studies based on elastic coherent scattering. From the diffraction point of view, inelastic and incoherent contributions are "background" effects. The fact that the wavelength of thermal neutrons is comparable to internuclear separations in molecules leads to an absence of vibrational selection rules. Selection rules in optical spectroscopy stem from the validity of the dipole approximation which is, in turn, based on the very large wavelength of light relative to the charge distribution changes associated with a molecular excitation. This approximation does not apply in thermal neutron scattering. Symmetry becomes less important except insofar as it relates to degeneracy. In optical terms, one may say that higher order multipolar contributions

TABLE 1: Neutron Scattering Cross Sections and Scattering Lengths[a]

element	coherent cross section (barns)	coherent scattering length (fermis, fm)	incoherent cross section (barns)	absorption cross section (barns)
hydrogen	1.8	−3.74	80.3	0.33
deuterium	5.6	6.67	2.0	0.0005
boron	3.5	5.30−0.213*i*	1.7	767
^{10}B (20%)	0.14	−0.1−1.066*i*	3	3835
^{11}B (80%)	5.6	6.65	0.21	0.006
carbon	5.6	6.64	0.001	0.005
nitrogen	11.0	9.36	0.5	1.9
oxygen	4.2	5.80	0.001	0.0002
fluorine	4.0	5.65	0.001	0.01

[a] From http://www.ncnr.nist.gov/resources/n-lengths/. Units: 1 fm = 10^{-13} cm, 1 barn = 10^{-24} cm^2.

* To whom correspondence should be addressed. E-mail: bshudson@syr.edu.

10.1021/jp004429o CCC: $20.00
Published on Web 03/24/2001

are important. It is the momentum transfer, **Q**, that dictates the effective wavelength of the interaction. Optical selection rules are approached for a given inelasticity with high energy incident neutrons and low scattering angle. These conditions minimize momentum transfer.

Another important aspect of neutron scattering is that thermal neutrons are highly penetrating radiation. This permits studies of hydrogen atom motions in compounds adsorbed on surfaces, in catalysts (including zeolites or metals), or otherwise "buried". Optical transparency is not required. Recent advances in neutron sources and spectrometer sensitivity permit studies of this type with small amounts of adsorbed materials.

Recent applications of inelastic neutron scattering spectroscopy have emphasized the fact that it is possible to compute the intensities of individual inelastic events from the normal mode eigenvectors. The frequency (and thus the inelasticity) of that event is given by the normal mode eigenvalue. For hydrogen containing molecules, the intensity of the event is proportional to the sum of squares of the hydrogen atom motions. Neglecting a Debye−Waller factor which is near unity at low temperature, the incoherent scattering intensity I_v of a fundamental transition of normal mode v with frequency ω_v is proportional to a sum over individual atoms $\Sigma_i \sigma_{(i)}(\mathbf{Q}\cdot\mathbf{C}_i^v)(\mathbf{C}_i^v\cdot\mathbf{Q})/\omega_v m_i$ where $\sigma_{(i)}$ is the incoherent cross section and m_i is the mass for atom i, $\mathbf{C}_i^v$ is the vector describing the motion of atom i in normal mode v, and **Q** is the neutron momentum transfer vector. The normal mode eigenvector for each mode is normalized: $\Sigma_i\ \mathbf{C_i^v}\cdot\mathbf{C_i^v} = 1$. For the spectrometers used in the experiments described here, the magnitude of the momentum transfer vector, **Q**, and the frequency are related by $\omega_v \propto \mathbf{Q}^2$. The value of $\sigma_{(i)}/m_i$ for hydrogen is so much larger than that for anything else that other atoms can be ignored. The simple expression $I_v \propto \Sigma_{i(H)}|\mathbf{C}_{i(H)}^v|^2$ thus applies for polycrystalline samples because orientation averaging simply leads to a factor of $^1/_3$.

Overtones and combinations are often important in inelastic neutron scattering even in the harmonic approximation. The intensity of a binary combination (one quantum excitation in each of modes u and v) or a two-quantum overtone (u = v) is given by $I_{uv} = \Sigma_i \sigma_{(i)}(\mathbf{Q}\cdot\mathbf{C}_i^u)(\mathbf{Q}\cdot\mathbf{C}_i^v)(\mathbf{C}_i^v\cdot\mathbf{Q})(\mathbf{C}_i^u\cdot\mathbf{Q})/\omega_{uv} m_i$. Given the same approximations used for the fundamental transitions, it is clear that these "two-quantum" excitations increase in intensity relative to the fundamental excitations in proportion to $\mathbf{Q}^2$ and thus become increasingly important at higher ω. The orientation averaging is not trivial in this case, however, because $\mathbf{C}_i^u$ and $\mathbf{C}_i^v$ are noncollinear vectors bear a fixed relative direction for each molecular orientation. Although this relative orientation may be determined by symmetry, it is, in general, a feature of the shape of the molecular potential energy surface. Combinations of one-quantum excitations of internal vibrations with external modes of motion leads to what are called "phonon wings" or "phonon sidebands". These also increase in relative importance with increasing frequency because they are also two-quantum combinations.

The spectra to be presented below were obtained using the TFXA or TOSCA spectrometers at the ISIS facility of the Rutherford Appleton Laboratory, Didcot, England or the FANS spectrometer at the NIST Center for Neutron Research, National Institute of Standards and Technology, Gaithersburg, MD. These and other neutron spectrometers and neutron source facilities are briefly reviewed at the end of this article after several examples of applications of this technique and the analysis of these spectra are presented. One experimental point should be mentioned here, however. In the experiments to be discussed, the final neutron energy is very small, ca. 10 cm^{-1} (in optical terms). The accessible vibrations are limited by the incident neutron energy. Neutrons that come from nuclear reactors have a distribution of energies that depends on the moderator temperature. There are neutrons in the thermal distribution with energies as high as 1000 or even 2000 cm^{-1} but with rapidly decreasing intensity. Spallation neutron sources, discussed below, have a high component of "epithermal" neutrons and can thus access high energy vibrations.

A brief bibliography on neutron scattering is given at the end of this article. This includes specialized review articles and review articles aimed at chemical applications as well as several monographs and text books. The physical concepts and equations presented below are given in all of these text books.

Applications to Molecules of High Symmetry: Dodecahedrane and Dodecaborane.

The nominally icosahedral molecule dodecahedrane, $C_{20}H_{20}$, provides a classic case for symmetry-based vibrational analysis. Under the I_h point group, the 114 normal modes of vibration are classified into $2A_g + 1T_{1g} + 2T_{2g} + 4G_g + 6H_g + 3T_{1u} + 4T_{2u} + 4G_u + 4H_u$ symmetry types. There are only 30 discrete vibrational frequencies because of the high average degeneracy. Of these, only the three T_{1u} modes are active in the infrared spectrum and only the two A_g and six H_g modes are active in the Raman spectrum. Thus, 19 of the 30 modes of vibration are unobservable by these optical methods so long as this molecule retains its high symmetry.

The inelastic neutron scattering spectrum of dodecahedrane[2] is shown in Figure 1 in dark blue. This spectrum was obtained with a sample of 260 mg of highly purified material contained in an aluminum sample cell that is ca. 4 cm in height, 2 cm wide, and 1−2 mm thick. In this spectrum, the IR and Raman active frequencies are indicated as red and green lines, respectively. The INS spectrum reveals many new features as expected. The relative simplicity and structured nature of the spectrum results from the high symmetry of this molecule. At the resolution of this spectrum, this symmetry is apparently preserved in the crystal where the site symmetry is T_h. Another factor contributing to the relative simplicity of this spectrum is the lack of phonon sideband intensity. This stems from the high mass of the molecule and relatively tight packing in the crystal. A contrasting case for a similar molecular structure is that of adamantane where phonon sidebands are quite strong.[3] The observation of intensity in the low-frequency features of the dodecahedrane spectrum reflects the fact that the carbon skeletal deformations result in motion of the hydrogen atoms because of their rigid attachment to the moving carbon atoms. The intensities of the observed features are roughly proportional to their degeneracy (as determined by the assignment to be described), with the nondegenerate A_g mode near 675 cm^{-1} being weak. However, this intensity scaling is only approximately the case, as is seen for the first two features near 500 cm^{-1}. These are both of H symmetry and thus 5-fold degenerate but differ in intensity by roughly a factor of 2.

The normal mode eigenvectors needed to calculate the INS intensities as outlined above can be computed from a normal mode calculation. Modern ab initio methods provide the most generally applicable method for performing such calculations. These methods first optimize the molecular geometry and then evaluate the second derivatives at the equilibrium position, usually using analytic derivatives. With the caveat that hydrogen stretches are highly anharmonic, it is well-established that such methods provide reliable values for vibrational frequencies for

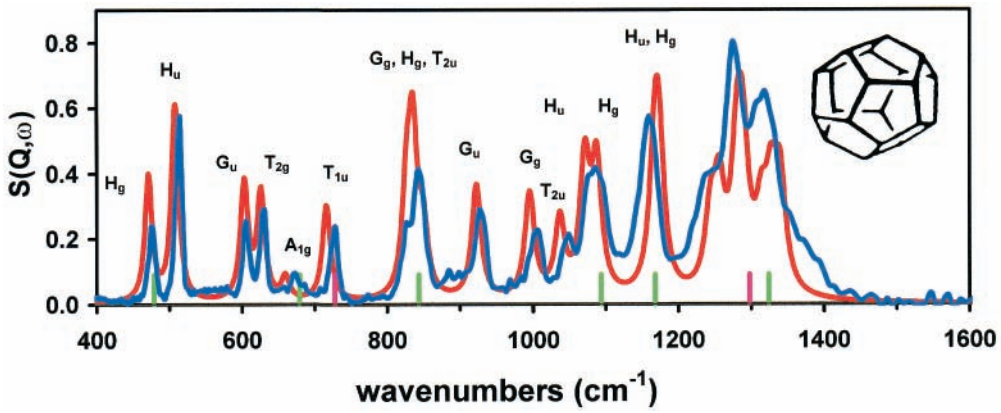

Figure 1. Inelastic neutron scattering spectrum of dodecahedrane obtained with TOSCA-1 at ISIS. The sample consisted of 260 mg of high purity polycrystalline material held in an aluminum container at approximately 15 K. The experimental spectrum is shown in blue; the computed spectrum based on a DFT B3LYP/6-31G** calculation in shown in red. (This convention is followed in all subsequent figures). The small vertical lines are the observed frequencies for Raman (green) and infrared (red) spectra (from Paquette et al. *J. Am. Chem. Soc*. **1983**, *105*, 5446; **1982**, *104*, 4503 and Bertz et al. *Can. J. Chem*. **1993**, *71*, 352). The symmetry labels refer to the I_h symmetry of the isolated molecule as determined by the DFT calculation. After 2, $S(\mathbf{Q},\omega)$ is defined in the texts listed in the Bibliography section.

small and medium size molecules.[4] Large basis set treatments that include anharmonicity or scaling procedures provide frequency agreement on the order of wavenumbers for isolated molecules. Even Hartree−Fock calculations are useful because they are nearly universally too high in frequency by a factor close to 9%, permitting a simple frequency scaling procedure.[4] The extent to which harmonic HF and DFT calculations provide adequate descriptions of normal mode eigenvectors is less often discussed. Comparison of calculated and observed infrared and Raman intensities is complicated by the requirement for adequate treatment of the response of the electrons to the motion of the nuclei. Comparison of frequency calculations for isolated molecules with data obtained for solutions or solids involves some relaxation of tolerance limits or some kind of treatment of the environment. There are fewer comparisons between theory and experiment for the low-frequency vibrations of large molecules. These vibrations are, presumably, more likely to be influenced by intermolecular interactions in solids. They may also be more anharmonic than higher frequency modes involving heavy atoms. A comparison of a calculated incoherent INS spectrum based on normal-mode frequencies and eigenvectors obtained from an isolated molecule calculation with experimental results obtained for a low-temperature solid is thus a test of the reliability of a large number of assumptions as to the importance of neglected effects. Recent advances in computational methods permit examination of each of these approximations.

Dodecahedrane is a good place to start this comparison of theory with experiment. As a hydrocarbon, the intermolecular interactions are expected to be small, perhaps exceeding only perfluorocarbons in this respect. Also, as a rigid cage structure, dodecahedrane has no internal vibrations in the low-frequency range where external vibrations ("phonons") occur (see Figure 10A). Furthermore, as noted above, the experimental spectrum has many resolved features and is not complicated by phonon wings.

The INS spectrum calculated for dodecahedrane on the basis of a DFT B3LYP/6-31G** calculation for the isolated $C_{20}H_{20}$ molecule is shown as the red line in Figure 1. The degree of agreement is sufficiently good that the assignment of the features is certain. Below 800 cm^{-1}, the spectral features correspond to individual vibrational modes of motion with the indicated symmetry labels. For these features, there are small but significant differences between theory and experiment with respect to frequencies and relative intensities. However, these discrepancies are sufficiently small that there is no chance that assignments could be inverted. Above 800 cm^{-1}, there are a few isolated transitions, and these are in similarly reasonable agreement with the calculation. Near 850 cm^{-1}, and also at higher frequency, there are sets of overlapping transitions. The full utility of incoherent INS with inclusion of intensity calculations is illustrated here in that the total intensity of these features is well represented by the calculated values, confirming the presence of the expected modes of motion despite their lack of resolution in the spectrum. The differences between theory and experiment in the line shapes for these cases of overlapping transitions are attributed to small frequency errors plus the lack of inclusion of overtones and combinations as discussed below. Examination of the spectrum of dodecahedrane at higher resolution with infrared and Raman methods has revealed splittings of the degenerate molecular species on the order of a few inverse centimeters and induction of intensity in the nominally forbidden modes. Specifically, for the T_h site symmetry, it is expected that all *g* symmetry modes will become Raman active, all *u* symmetry modes will become IR active, and the highest symmetry is only 3-fold degenerate. The pattern of the splitting and induced intensity is consistent with this group theoretical analysis, and this serves to further confirm the spectral assignments. The calculation of the splitting is discussed below.

The boron hydrides, such as the icosahedral $B_{12}H_{12}^{-2}$ ion, provide interesting challenges experimentally for neutron scattering spectroscopy because of the absorption of neutrons by ^{10}B, the minority (20%) isotope of this element. In natural abundance boron hydride samples, this results in a penetration depth of the neutron beam on the order of 1 mm. For a backscattering spectrometer such as TFXA or TOSCA at ISIS, this is not a particular problem in principle, but in practice, the signal-to-noise obtained is not as good as for a hydrocarbon. The spectrum of $Cs_2B_{12}H_{12}$ is shown in Figure 2.[5]

The $B_{12}H_{12}^{-2}$ ion has nominal icosahedral symmetry. In this symmetry, the 66 vibrations of $B_{12}H_{12}^{-2}$ fall into 18 degenerate groups of the type $2A_g + T_{1g} + 2G_g + 4H_g + 3T_{1u} + 2T_{2u} + 2G_u + 2H_u$. The $3T_{1u}$ modes are IR active, whereas the $2A_g$ and $4H_g$ modes are Raman active. The other nine vibrations are silent. The INS spectrum of $Cs_2B_{12}H_{12}$ in Figure 2 is compared with the results of a DFT B3LYP/6-31G** calculation. The calculation is for the isolated ion. The agreement is sufficiently good that one can, for the most part, assign the

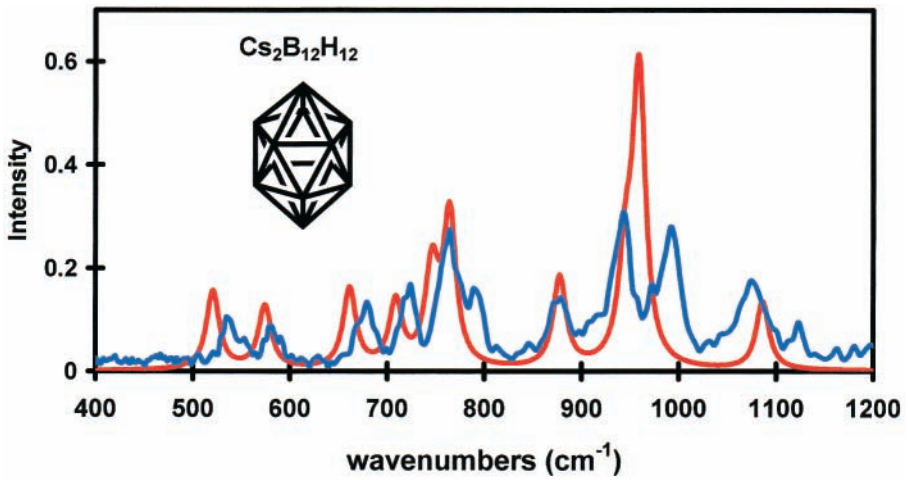

Figure 2. Observed (blue) and calculated (red) inelastic neutron scattering spectra of cesium dodecaborane. The sample was 1 gm at ca. 15 K. The large peak at ca. 950 cm^{-1} has four individual (degenerate) components. Reference 5.

vibrational features. The major exception is in the 900−1050 cm^{-1} spectral region. The calculation correctly positions the G_g vibration at 878 cm^{-1} and the T_{1u} vibration is placed reasonably at 1086 cm^{-1} (observed in IR at 1070 cm^{-1} in agreement with the INS feature), but there are four calculated transitions that are too close together in frequency to be in agreement with experiment. These are G_u at 945.2 cm^{-1}, H_g at 957.7 cm^{-1}, T_{1g} at 959.6 cm^{-1}, and H_u at 959.8 cm^{-1}. These four individual degenerate transitions are calculated to have approximately equal intensity in the INS spectrum. Their superposition results in the single feature near 960 cm^{-1}. Comparison of the observed spectrum and that calculated but displayed with a higher resolution shows that the G_u vibration is correctly predicted in frequency. Comparison of the intensities shows that one of the other three vibrations is calculated too high in frequency and the other two are calculated too low by about 30 cm^{-1}. The origin of these discrepancies is not clear at the present time. It is, however, possible to be a bit more specific as to the nature of these discrepancies. The H_g vibration is observed in the Raman spectrum at 949 cm^{-1}, consistent with this transition being calculated too high in value. Movement of this band down to 949 cm^{-1} results in a composite $G_u + H_g$ peak with the appropriate intensity (relative to the two bands at 880 and 1080 cm^{-1} above and below the region of interest) and leaves the $T_{1g} + H_u$ bands with the appropriate intensity to comprise the higher frequency feature near 980−985 cm^{-1}, 20−25 cm^{-1} higher than calculated. Possible origins for the discrepancy between theory and experiment in this case include lack of an adequate basis set for this anionic species or the influence of the crystalline environment. In regard to the later, it is interesting to note that the crystal structure determination for the potassium salt gives B−B bond lengths of 1.755 and 1.780 Å in the T_h symmetry cell.[6]

An Example of Coherent Scattering: Hexafluorobenzene

When a molecule does not contain hydrogen, it is necessary to include coherent scattering in the description of the transition intensities. In many cases, this is the dominant scattering mechanism. The empirical difference between coherent and incoherent scattering is most easily described in terms of elastic scattering. Coherent elastic scattering is usually called diffraction. There are constructive and destructive interactions between the amplitudes corresponding to different regions of the sample and, thus, at the atomic level, between different atoms (or different nuclei for neutrons). This results in Bragg scattering and Bragg peaks, strong scattering in particular directions. Incoherent scattering results from what is effectively disorder in the crystal. This results in a loss of phase between the scattering components in different regions of the material and in isotropic scattering. In the optical case, for a beam of light propagating through a gas or liquid, this corresponds to forward beam propagation (coherent scattering) and Rayleigh scattering because of density (and thus refractive index) fluctuations. Raman scattering is also incoherent because of the random phase of the scattering from molecules at different positions.

Table 1 gives the values for the coherent and incoherent scattering cross sections for several common elements. The natural abundance isotopic form is given unless noted. An example of an inelastic coherent neutron scattering experiment is provided by the case of C_6F_6. In this case, the incoherent scattering is negligible for both elements and the coherent scattering lengths are roughly equal and of the same sign. The expression for one-phonon inelastic coherent neutron scattering using the same notation as above is

$$I_v = 4\pi|\Sigma_i\, b_{(i)} \exp(i\mathbf{Q}\cdot\mathbf{R}_i)\, (\mathbf{C}_i^v\cdot\mathbf{Q})/(\omega_v m_i)^{1/2}|^2$$

The analogy with the incoherent expression can be recognized by noting that the cross section for incoherent scattering, σ_{inc}, is given by $4\pi b_{inc}$.[2] The corresponding coherent cross section is $4\pi b_{coh}$.[2] The difference is that this expression for coherent scattering involves a coherent scattering length (which may be negative), includes cross terms between different atoms involving atomic displacements in mode v, $(\mathbf{Q}\cdot\mathbf{C}_i^v)(\mathbf{C}_j^v\cdot\mathbf{Q})$, and includes an atomic position term, $\exp(i\mathbf{Q}\cdot(\mathbf{R}_i - \mathbf{R}_j))$. This last factor gives rise to the structural information in elastic scattering, i.e., neutron diffraction. This vanishes in incoherent scattering where $\mathbf{R}_i - \mathbf{R}_j = \mathbf{R}_i - \mathbf{R}_i = 0$. Only single-atom terms appear in the incoherent case, but in coherent scattering, it is scattering from pairs of atoms that is observed. The orientation averaging for this coherent scattering is again nontrivial as it is for combination and overtone scattering.

Fluorocarbons have several interesting peculiarities in terms of their structural chemistry. Some of these are the preferred gauche conformation of 1,2-difluorethane and the greater stability of *cis*-1,2-difluorethylene in comparison to the trans isomer. The fluoromethanes increase in average C−F bond strength as the degree of fluoroination increases in the series CH_3F, CH_2F_2, CHF_3, and CF_4. The opposite trend is seen for chlorine. We were struck by the large degrees of discrepancy

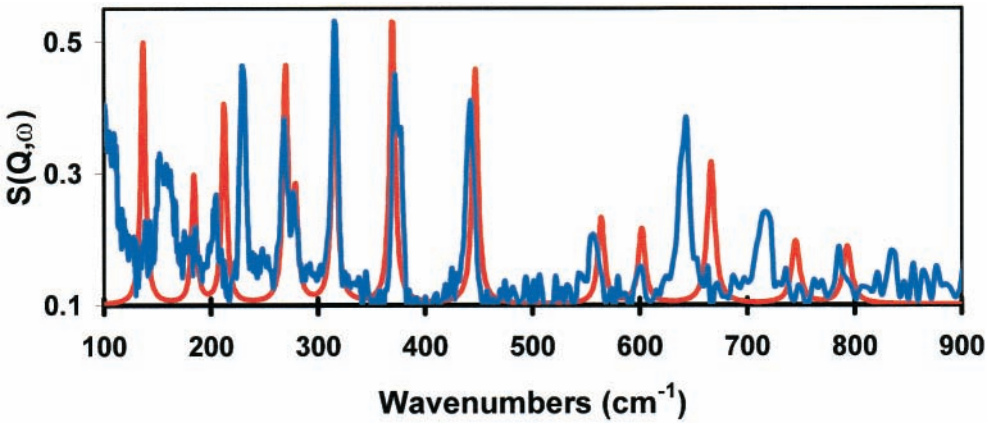

Figure 3. Observed (blue) and calculated (red) inelastic neutron scattering spectra of polycrystalline hexafluorobenzene. In this case, the sample was ca. 10 gm. After 7.

between calculated and observed vibrational frequencies for hexafluorobenzene.[7] With a B3LYP/6-311+G* basis calculation the root-mean-square (rms) deviation between theory and experiment for the 11 infrared or Raman active modes of C_6F_6 is 8 cm^{-1}. This is typical of the degree of agreement observed for a variety of hydrocarbon species. Comparison of the frequencies calculated for the nine IR and Raman inactive modes with the values reported on the basis of studies of crystalline C_6F_6 yields an rms deviation of 49 cm^{-1} for the same calculation. Two of these vibrations (ν_{17} at 137 cm^{-1} and ν_{12} at 1330 cm^{-1}) are quite accurately calculated (deviation of 1 and 7 cm^{-1}, respectively), but the other seven inactive modes differ in some cases by as much as 78 cm^{-1}, with 64 and 49 cm^{-1} deviations also found. An MP2 calculation with a 6-31+G-(d′) basis gives an rms deviation of 166 cm^{-1} for these nine inactive modes with some of the calculated frequencies being entirely out of line from those calculated by other methods. Analysis of the INS spectrum (Figure 3)[7] shows that five of the seven "high deviation" inactive modes were incorrectly assigned in the analysis of weak features in the optical spectra. This reassignment of the experimental results brings the rms deviation for the nine inactive modes down to 30 cm^{-1}, with the large deviation cases of 78, 64, and 49 cm^{-1} being reduced to 1, 21, and 4 cm^{-1}, respectively. A bigger basis (aug-cc-pVTZ) gives an rms deviation of 20 cm^{-1} for the new assignment and 42 cm^{-1} for the original optically based assignment.

The spectrum of hexafluorobenzene shown in Figure 3 required a sample of 10 g and a data accumulation time of 12 h. The dodecahedrane sample on the same version of the TOSCA spectrometer would have yielded the same signal-to-noise in a couple of hours with 260 mg sample. This illustrates the practical aspects of dealing with a non-hydrogen containing compound and the need for brighter neutron sources.

The *n*-Alkanes: Dispersion in a Single Chain.

The low-frequency vibrational spectroscopy of the linear *n*-alkanes has a long and interesting history.[8−11] The most famous series of low-frequency modes of these compounds are the longitudinal acoustic modes or "LAMs". These vibrational normal modes involve the longitudinal motion of the *n*-alkane atoms along the molecular axis direction of the fully extended chain. For an *n*-alkane with N carbon atoms, there are $N - 2$ LAM modes. CCC angle bending is the major coordinate involved, but there may be some contribution of the C−C stretch. These LAMs may be classified in terms of the phase difference, ϕ, between the motions of the adjacent translationally equivalent CH_2-CH_2 groups. Zero phase angle between adjacent groups corresponds to translation of the entire chain and thus to translation. This has no restoring force and so occurs at zero frequency, giving rise to the "acoustic" designation. This phase difference between unit motions can be transformed into an equivalent wavelength or wavevector via $k = 2\pi/\lambda = 2\phi/a$. The maximum value of k is given by $2\pi/a$ where a is the lattice spacing for the periodic structure. The maximum value of ϕ is π. The LAM modes exhibit a smooth dispersion behavior when plotted as a function of ϕ. The longest wavelength (lowest k and ϕ) mode that occurs with finite frequency is the LAM-1 or "accordion" mode. In this mode, all of the atoms on one end of the chain move in one direction and all of the atoms at the other end of the chain move in the other direction. The atom in the center of the chain is undisplaced. All of the bond angles contract (or expand, depending on the phase of the oscillation). This LAM-1 vibration is observed in Raman scattering for hexadecane at 150 cm^{-1}. The higher order LAM modes have an increasing number of nodes in displacement pattern. For $n = 24$, the LAM-1 mode is observed at 104 cm^{-1}. The wavelengths for these modes are proportional to the chain length. The dispersion curve for the infinite chain can be followed to higher k (or ϕ) by examination of shorter length chain hydrocarbons based on the argument that the higher order LAM mode of an infinite chain will be the same as that for a finite chain whose length matches the wavelength of the infinite chain mode. For $n = 8$ LAM-1 is at 281 cm^{-1}. The dispersion observed in going from 24 to 16 to 8, i.e., 104, 150, and 281 cm^{-1}, is not linear. This type of analysis has been used to establish the form of the dispersion curve for the *n*-alkanes and, by implication, for polyethylene. This analysis is based on neglect of end effects which is a good approximation for the longer *n*-alkanes. This leads to the conclusion that the LAM mode dispersion curve exhibits a linear increase at small ϕ, reaches a maximum value of ca. 525 cm^{-1} at intermediate ϕ (near $\pi/3$), and then decreases back toward zero as $\phi \rightarrow \pi$. This dispersion behavior is illustrated by simple models that include only angle bending when these are treated in the infinite chain limit.[11] The main features are thus not determined by end effects. However, to make a quantitative determination of this dispersion behavior it is necessary to observe higher order LAM modes for finite chains and to correct for these end effects.

Higher order LAM modes with larger ϕ correspond to shorter wavelength periodicities. If such vibrations are probed with long wavelength radiation, the dipole moment change induced by this motion in one region of the chain tends to be canceled by the dipole moment change of opposite sign in another region.

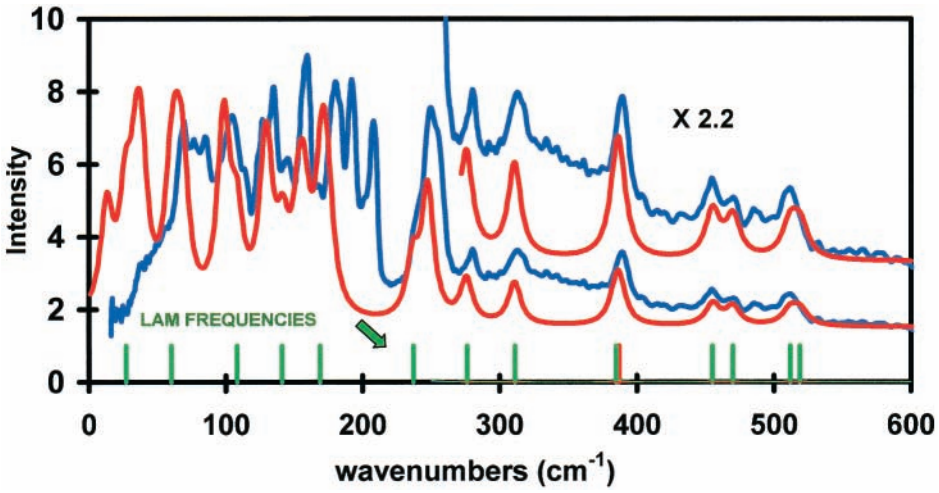

Figure 4. Observed (blue) and calculated (red) inelastic neutron scattering spectra of polycrystalline *n*-hexadecane. The sample was ca. 1 gm. Both spectra have been multiplied by 2.2 to give the raised traces at the right. The small lines at the bottom give the frequencies calculated for the longitudinal acoustic modes (LAM) vibrations of this molecule. These are in green except for one that is in red because of proximity to another line. After 9.

Similar behavior is expected and observed for the polarizability derivatives. In the infinite chain limit where translational symmetry applies, this cancellation is exact and corresponds to restriction of the LAM excitations to the $k = 0$ limit appropriate to electromagnetic radiation of long wavelength. As a result, only the low order LAM modes are observed for a given *n*-alkane. It has not been possible to observe the higher order LAM modes. This has prohibited determination of their frequencies, and this obscured the magnitude of the end effects and made comparison with ab initio theoretical calculations of limited utility.

Inelastic neutron scattering is not restricted by these effective selection rules. The INS spectrum of hexadecane is shown in Figure 4. The vibrations in the region from 250 to 525 cm^{-1} are LAM modes. In the lower frequency region, there are out-of-plane bending modes and also external vibrations. The highest frequency out-of-plane motion is the methyl rotation near 250 cm^{-1}. With 16 carbons, this molecule has 14 LAM modes. LAM-1 is at 150 cm^{-1} as determined from optical measurements. LAM-2 is at ca. 280 cm^{-1} just above the strong methyl rotation peak. The next few LAM modes increase in frequency to 513 cm^{-1} (LAM-5 and LAM-6) and then decrease in frequency until LAM-10 overlaps the methyl torsions. Figure 5A shows this dispersion behavior for all of the *n*-alkanes with 5−25 carbons. The smooth curve that is drawn through the data is the result of a calculation by Okada[11] for a model for the infinite chain in which the bond lengths are fixed, the CH_2 groups are considered as point masses, and only the CCC bond angle deformation contributes to the potential function. The force constant/mass ratio is adjusted to produce a maximum frequency of 525 cm^{-1} as appears to be appropriate for the infinite chain. Figure 5B shows the same results for these *n*-alkanes with $n =$ 5−25 as calculated using density functional methods (B3LYP/6-31G**). In this case, the data extends to higher ϕ than the experiment where at low frequency the experimental LAM features are overlapped by the out-of-plane modes. The subsequent LAM modes for hexadecane beyond LAM-10 are calculated to be at 169, 108, 60, and 27 cm^{-1} for LAM-11 through LAM-14. That these are reliable estimates is confirmed by the degree of agreement shown for the assigned features in Figure 5C. This general procedure has been extended to the actual case of polyethylene where, for deuterated polyethylene, the dispersion curve has been measured directly.[10]

Deuterium "Masking" and Oriented Samples: *n*-Hexadecane in Urea Inclusion Crystals.

The problem of the disentanglement of the low-frequency LAM modes from the out-of-plane bending modes of *n*-alkanes has been approached by a method that illustrates the utility of deuterium substitution in composite molecular crystals. This procedure involves *n*-alkane urea inclusion crystals.[12] These crystalline materials are helical arrangements of urea that surround enclosed *n*-alkane chains in their all-trans extended form in hexagonal arrays. The parallel helical channels filled with *n*-alkanes lie along the *c* axis of the crystal. Large crystals are easily grown from solution. These crystals are macroscopic hexagons that can be aligned parallel or perpendicular to the neutron momentum transfer vector. This permits separation of those vibrations in which the atoms move parallel to the crystal *c* axis or perpendicular to that axis.[13] These two cases correspond to longitudinal and transverse modes of motion for the *n*-alkane. A difference spectrum of *I*(parallel) − *I*(perpendicular) will have positive features for longitudinal motions and negative features for transverse motions. A difference spectrum of this type is shown in Figure 6. The known longitudinal and transverse modes exhibit the expected behavior. The success of this experiment depends on the fact that the urea can be deuterated. The INS spectra are then dominated by the *n*-alkane hydrogen atoms.

Hydrogen-Bonded Lattices: Oxamide.

Hydrogen-bonded complexes provide examples of structures that can most fruitfully be investigated using INS because of the particular relevance of H atom motion to the spectral intensity. On the other hand, such structures provide extra challenges in the comparison of theory with experiment. The use of an isolated molecule calculation for the description of the motions of H-bonded lattices gives results that disagree greatly from what is observed. There are at least two reasons for this. One is the obvious fact that hydrogen bonding restricts the motion of the hydrogen atoms. The other factor, especially important for peptides, is that hydrogen bonding results in significant structural changes including the C═O bond length (which increases) and the C−N bond length (which decreases) on hydrogen bond formation.[14]

The degree of disagreement between an isolated molecule calculation and experiment is especially large for the INS spectra

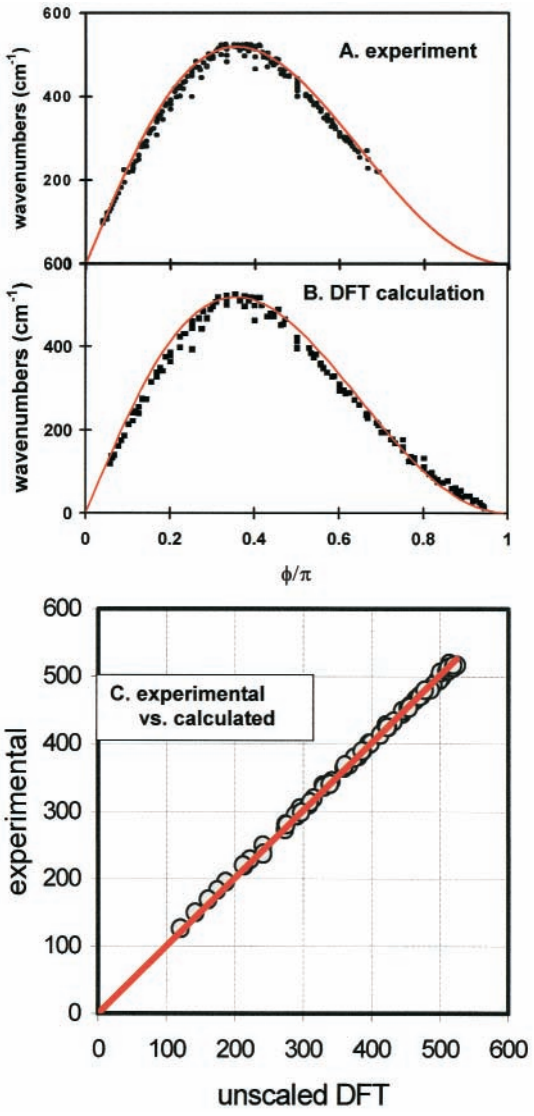

Figure 5. *n*-Alkane dispersion behavior. (A) The experimental longitudinal acoustic mode (LAM) vibrational frequencies of the *n*-alkanes with 5−25 carbons plotted as a function of the LAM phase angle, ϕ. (B) The same but as obtained from DFT calculations. (C) A comparison of calculated and observed LAM frequencies for the *n*-alkanes. After 9.

where hydrogen atom motions are emphasized. One approach that has been used in such cases consists of adjusting the force field for the molecular unit so as to fit INS frequency and intensity data. In such treatments, the phonon spectrum is treated empirically and then folded in with the internal molecular vibrations to produce the phonon sidebands.[15] Overtones and combinations of the internal motions are calculated in the harmonic approximation. These, and the phonon sidebands, are added to the spectrum with increasing relative intensity at high **Q**. A Debye−Waller factor is added. This Debye−Waller factor is different for the internal motions and the phonon sidebands.[16]

Such an approach, although potentially reproducing the data, does not test an ab initio calculation. It also misses degrees of freedom that may be important. The strength of hydrogen bonds is such that there may be significant dispersion of the molecular vibrations in the crystal. This will result in broadened lines in the INS spectrum with the extent of broadening being dependent on the degree of dispersion (and thus on the particular vibration in question). It is important to note in this context that incoherent INS averages over the Brillouin zone rather than being limited to $k = 0$, the zone center, as is the case for optical spectroscopy. In fact, incoherent INS emphasizes the large k edge of the zone because of the higher density of states. This results in the fact that the frequencies observed in incoherent INS and optical spectroscopy are be slightly different, the degree of difference being dependent on the extent of dispersion of the particular vibration. This also means that the INS lines will be broader than optical lines even when not limited by spectrometer resolution. However, for internal vibrations of weakly interacting molecules the degree of dispersion is quite small, i.e., the frequency difference between the zone center and zone edge is only a few inverse centimeters. For these "typical" molecular vibrations, the limiting factor is presently spectrometer resolution. However, external vibrations (phonons) and the nominally internal vibrations of molecular crystals with strong intermolecular interactions exhibit much larger dispersion and significant broadening.

Crystalline oxamide $O(HN_2)C-C(NH_2)O$ illustrates these features.[17] The analysis of this INS spectrum illustrates two approaches to this problem. One approach is to perform a calculation for a cluster model of the solid. For oxamide, this is facilitated by the fact that the $Z = 1$, planar, centrosymmetric structure of the hydrogen-bonded lattice permits a two-dimensional model to be implemented. Figure 7A compares the experimental spectrum with that resulting from a pentamer model in which a central oxamide molecule is surrounded by four hydrogen-bonded neighbors in a plane. This planar pentamer array is treated as a super molecule for which all of the normal modes are calculated. The INS spectrum is then computed by inclusion of the motions of only those atoms that are in the central oxamide unit (the hydrogen-bonded atoms). The motion of these four H atoms is distributed over many of the modes of the complex. The intensity of each frequency is set proportional to the sum of squares of the contribution of the central molecule hydrogen atoms to the normal mode eigenvector. Intensity is placed at the appropriate frequency with an area given by the sum of squares of the H-atom motion and a width dictated by the instrument resolution at that frequency. This is summed to produce the resulting spectrum.

This comparison is discussed in detail elsewhere,[17] but a few points should be noted here. First, most of the intensity in the region from 0 to 200 cm^{-1} is due to external motions of the molecule in the lattice. The large width of this intensity distribution reflects the strength of hydrogen bonding in this material. The sharp feature at 120 cm^{-1} is, however, due to an internal mode. Second, this calculation completely misses the relatively large feature just above 900 cm^{-1}.

This model captures the effect of hydrogen bonding on the molecular structure, and it constrains the NH_2 groups appropriately. It also provides a "low resolution" picture of the intermolecular coupling of the vibrational degrees of freedom that lead to dispersion. This is shown as the artificially narrowed plot shown in green at the bottom in Figure 7A. This gives the distribution of intensity into the modes of the pentamer with resolution adequate to show that each major feature consists of several individual transitions even at the level of fundamental transitions for this pentamer. These correspond to modes that consist of various centrosymmetric couplings of the internal modes. Because the pentamer is comprised of three molecules in each of two dimensions, this corresponds to three points in k space with phase angles between molecular vibrations of 0, $\pi/2$, and π for each crystal direction in the molecular plane. The splitting of these features is relatively large in this case because of the strength of hydrogen bonds.

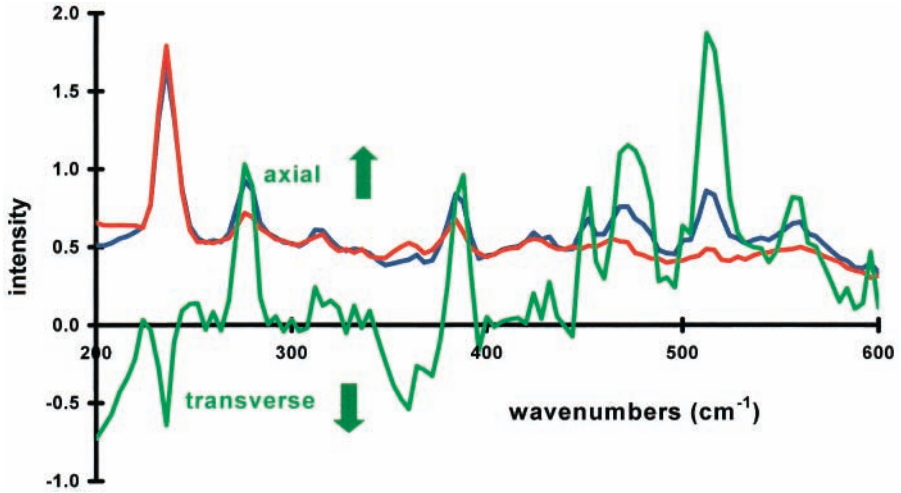

Figure 6. Inelastic neutron scattering spectra of *n*-hexadecane in urea inclusion complexes oriented with the crystal *c* axis parallel and perpendicular to the neutron beam and the difference spectrum. The blue curve shows the spectrum for axial orientation of the crystals with respect to the beam; the red curve, for transverse orientation. The green curve is the difference, axial − transverse. LAM modes give rise to positive features in the (green) difference spectrum. The feature near 235 cm^{-1} is dominated by the methyl torsions and is negative in the difference spectrum consistent with the transverse nature of this mode. The highest frequency LAM mode is seen near 520 cm^{-1} and is axially polarized as expected. After 13.

At this point, the spectrum does not include overtones or combinations. Phonon sidebands, a special kind of combination, are also not included. The spectrum of the overtones and combinations of the internal vibrations can be calculated in an approximate way. The frequencies of these features can be computed as multiples or sums of the fundamental frequencies in the harmonic approximation. The intensity for a combination transition involving modes u and v (u = v is an overtone), using the same notation as above, is given by $\Sigma_i(\mathbf{Q}\cdot\mathbf{C}_i^{u})(\mathbf{Q}\cdot\mathbf{C}_i^{v})(\mathbf{C}_i^{v}\cdot\mathbf{Q})(\mathbf{C}_i^{u}\cdot\mathbf{Q})/\omega_{uv}$ where the summation index *i* labels the hydrogen atoms. This is approximately $\mathbf{Q}^4\Sigma_i|C_i^{u}|^2|C_i^{v}|^2/\omega_{uv}$. Because $\mathbf{Q}^2$ is proportional to ω to a good approximation for this spectrometer, this reduces to $\omega_{uv}\Sigma_i|C_i^{u}|^2|C_i^{v}|^2$. Thus, the overtone and combination intensity increases with frequency. The calculated overtone and combination intensity is shown in Figure 7B as the light green trace. It is clear that this accounts for much of the intensity observed slightly above 900 cm^{-1}. This treatment for combinations is approximate because it should take into account the relative directions of the motion of atom *i* in modes u and v, i.e., the dot product with the momentum transfer vector might be zero for one mode whenever it is unity for the other. Also, the orientation averaging of this dyadic quantity must be computed numerically. This refinement is in progress.

To include the phonon sidebands, it is necessary to either compute[18] or to model the phonon spectrum.[15] The resulting intensity distribution can then be treated as combinations with the internal modes. Figure 7B shows the results of an empirical treatment for oxamide as the magenta line. In this treatment, the phonon spectral intensity is represented as a series of features placed sufficiently close together that when given a width they form a continuous distribution of intensity. These features are then treated as combinations with all of the internal modes with increasing intensity at higher frequency. In this case, the resulting distribution is essentially a rather bumpy baseline. It is seen that with inclusion of this contribution the broad feature above 900 cm^{-1} is now computed with too much intensity. This treatment is approximate because it does not account for the relative direction of the motions of the atoms because of internal motions and external motions. This is equivalent to the assumption that the phonon motion is isotropic, as is the case in a cubic crystal.[19]

Another approach to the treatment of the INS spectra of solids is a molecular dynamics computation of the density of states using a potential function that is computed from a periodic DFT quantum mechanical treatment. This approach has also been applied to the case of oxamide.[17] This treatment used the CASSTEP periodic DFT method that is based on plane-wave basis sets.[20] Periodic DFT treatments using atom-centered basis sets have also been developed (DMol^3).[21] The application of this last method in a harmonic approximation accurately describes the splitting of the degenerate lines of dodecahedrane seen in the IR and Raman spectra because of the T_h site symmetry. It also improves the degree of agreement between the calculated and observed INS spectra for this symmetric hydrocarbon.[22]

Co-crystals: Imidazolium Hydrogen Maleate and Urea Pimelonitrile.

A particularly interesting series of materials for the study of hydrogen bonding is provided by the stoichiometric hydrogen-bonded complexes known as co-crystals. Two examples of these are illustrated in Figures 8 and 9. The imidazolium hydrogen maleate case is of interest because of the very short O−H−O distance in the hydrogen maleate anion and the probable equal distance of the H atom to the two oxygen atoms.[23] This is an example of a molecular recognition motif that has been used in the design of enzyme inhibitors. The urea pimelonitrile complex is an example of a series of planar complexes with differing numbers of carbon atoms in the dinitrile component.[24] The urea molecules are oriented with their C═O groups either parallel or antiparallel in the plane of the sheets. This is an example of a crystal engineering motif potentially useful for nonlinear optical materials development. Another interesting case is that of the planar cyclic complex formed by six molecules of 1,3-cyclohexanedione in its enol form that surround a molecule of benzene.[25] Like clathrates, this is a model for the hydrophobic effect.

From the point of view of the subject of this article, co-crystals are of interest because they permit a very detailed test of a proposed potential energy surface. If we schematically represent the empirical formula of these complexes as AHB, where "H" represents all of the exchangeable protons involved

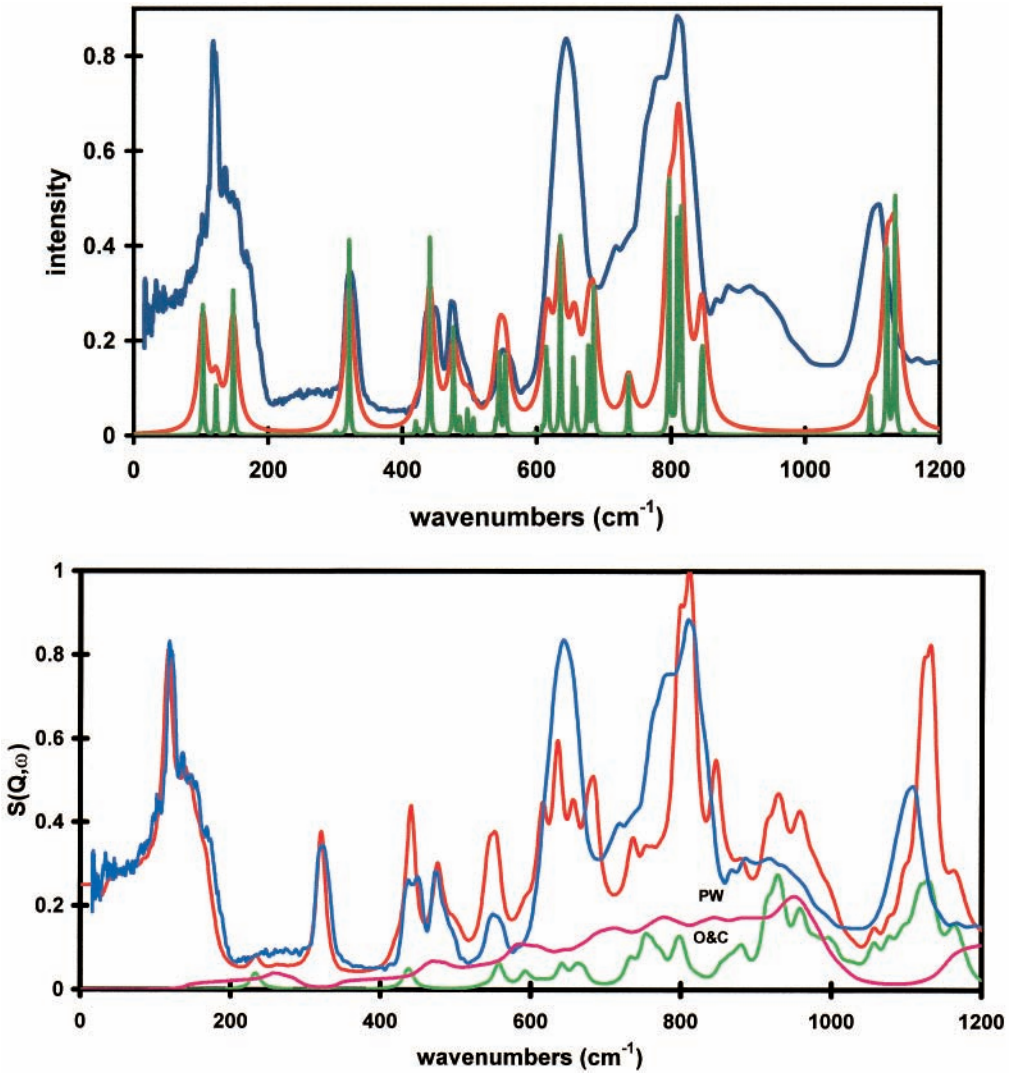

Figure 7. (A) Calculated (red) and observed (blue) inelastic neutron scattering spectrum of oxamide, O═C(NH2)-C(NH2)═O. This calculation is a Hartree−Fock computation on an oxamide pentamer scaled by a factor of 0.93. The green trace at the bottom is based on the same calculation as the red trace but is drawn with an artificially narrow resolution function in order to exhibit the complex nature of many of these vibrational features even at the level of fundamental transitions. (B) The observed (blue) and calculated (red) inelastic neutron scattering spectra of oxamide. The calculated spectrum now includes the contributions from overtones and combinations (green "O&C" trace at the bottom) and phonon wings (magenta "PW" trace). The red trace at the top is the sum of these plus the fundamental intensity shown in A. After 17.

in H bonds, then each of the three components A, H, and B can be independently deuterated yielding eight possible H/D complexes in all. Of greatest interest, perhaps, is the case where A and B are deuterated and the hydrogen-bonded components are protonated by exchange. Then the INS spectrum emphasizes the H-bonded components. The ability of a harmonic force field to describe the dynamics of the complex in all of its isotopomeric forms is a detailed test of the ability of an ab initio method to describe the entire system. Because vibrational spectra are very sensitive to structure, such a comparison between theory and experiment serves as a detailed test of structure as well.

The analysis of the spectra presented in Figures 8 and 9, and indeed the collection of these spectra, is still at a preliminary stage. It is clear, however, that the intermolecular hydrogen bonds that are part of the repeating unit of the crystal give rise to strong features in the spectra and that the analysis of these spectra will lead to detailed tests of the ability of ab initio and DFT methods to describe hydrogen bonding. The planar nature of the lattice of many of these composite materials permits modeling, at least initially, with two-dimensional clusters, as was done for oxamide.

Phonons

The external motions of molecules in a lattice are determined by the intermolecular forces that hold the units together and the repulsive forces that prevent their overlapping. Figure 10 shows the phonon region for several of the systems discussed above. In the case of oxamide, this spectral region is compared with the low-frequency features obtained from the pentamer calculation. In the RHF and DFT calculations for the pentamer, there are four vibrations in this frequency region: the a_u internal torsion is the lowest in each case, followed by the two b_u symmetry relative translations (x and y), and then the a_g in-plane rotational libron. In the RHF calculation, the a_u torsion and lowest frequency translational phonon are nearly degenerate and thus form the relatively strong peak. These are separated in a DFT calculation. The experimental spectrum appears to consist of a rather broad feature that begins at the lowest frequencies studied, rises in intensity to a maximum near 150 cm^{-1}, and then drops to near zero just below 200 cm^{-1}. On this broad feature is superimposed a sharp feature. This overall pattern is explained as a strongly dispersive set of phonons on which the nondispersive internal a_u torsion is superimposed. The

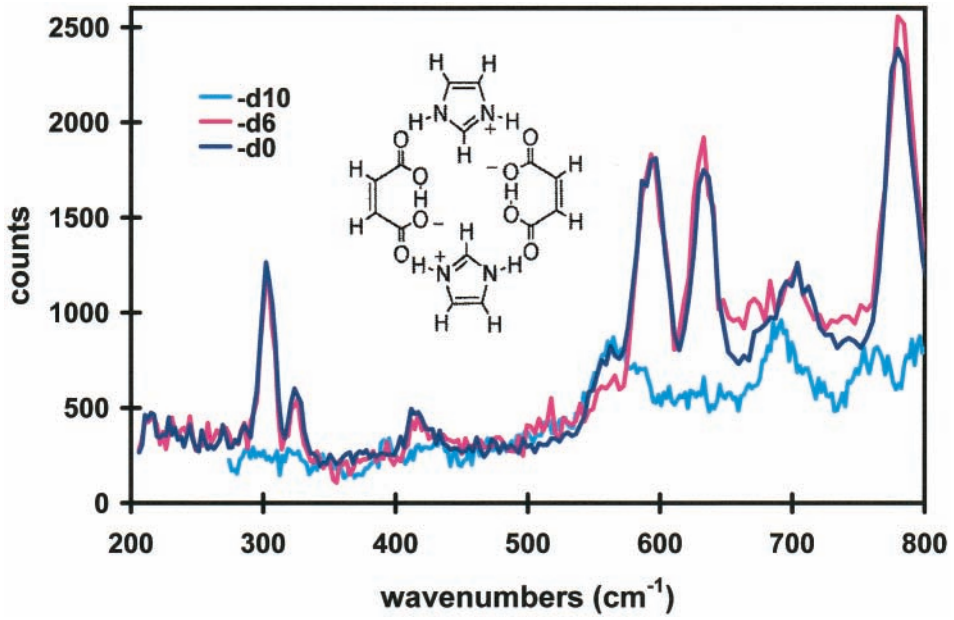

Figure 8. Inelastic neutron scattering spectrum of the imidazolium hydrogen maleate cocrystal in three isotopomeic forms. The dark blue spectrum is for the fully protonated form ($-d_0$). The red trace is for the form in which the six exchangeable protons have been replaced by deuterium ($-d_6$). The bottom blue trace is for the case where the 10 nonexchangeable CH protons are replaced by deuterium and the six exchangeable protons are H ($-d_{10}$). This $-d_{10}$ trace identifies the motions of the hydrogen-bonded hydrogens. Comparison of the $-d_0$ and $-d_6$ traces with the $-d_{10}$ trace shows that some of the vibrations (such as those near 300 cm^{-1}) are clearly dominated by the CH atom motions and that the H-bonded motions are primarily near 580 and 690 cm^{-1}. These spectra were obtained at NCNR with the new FANS spectrometer.

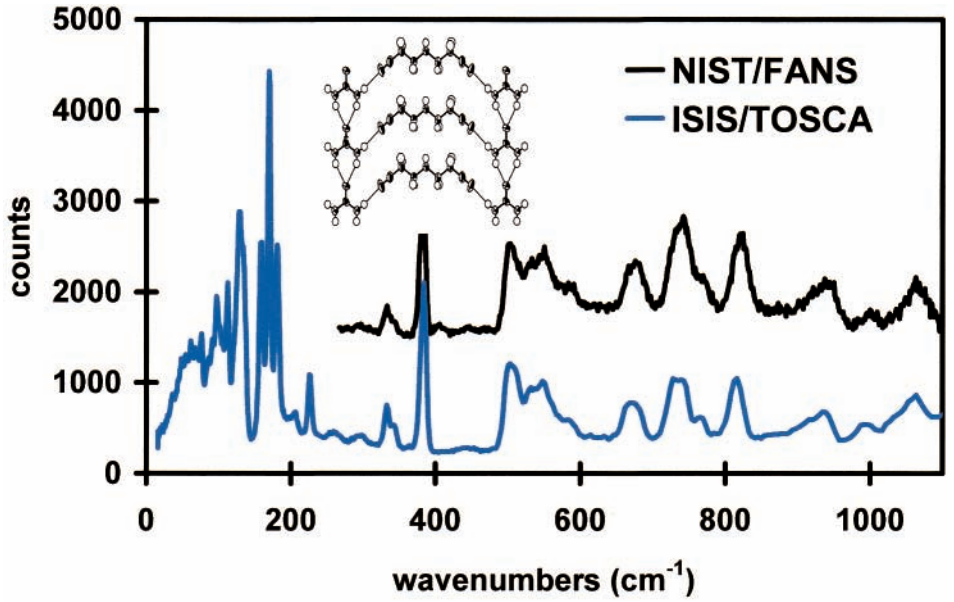

Figure 9. Inelastic neutron scattering spectra of the pimelonitrile urea cocrystal. The lower blue trace was obtained with TOSCA-1. The upper black trace was obtained with the FANS spectrometer at NIST.

large width of the phonon feature is due to the strong hydrogen bonding in this material.

The phonon spectra of the other materials have as yet not been investigated. The most efficient way to simulate these spectra, and at the same time to include the effects of intermolecular interactions on molecular structure and dynamics, is using periodic DFT methods. There are two available implementations of periodic DFT that include the capability for geometry optimization in the periodic lattice and evaluation of second derivatives for harmonic normal-mode analysis. One of these is CASTEP[20] and the other[21] is DMol[3]. These differ in the form of the basis sets used (plane wave and numerical grid atom centered, respectively). Calculations using super-molecule clusters with these methods have been found to be useful in their ability to describe phonon motions in an ab initio way.

Neutron Facilities and Spectrometers

Most of the experiments presented in this brief review were performed at the Rutherford Appleton Laboratory, Chilton, Didcot, UK.[26] The neutron facility at RAL is called ISIS.[27] This is a spallation neutron source. In such a neutron facility, high energy (ca. 1 GeV or more) protons strike a heavy element target and induce nuclear fission and the release of neutrons. The number of neutrons released per incident proton increases with the proton energy and is about 20−30 for 0.8 GeV protons. The protons are produced in tight bunches, and thus, the neutrons

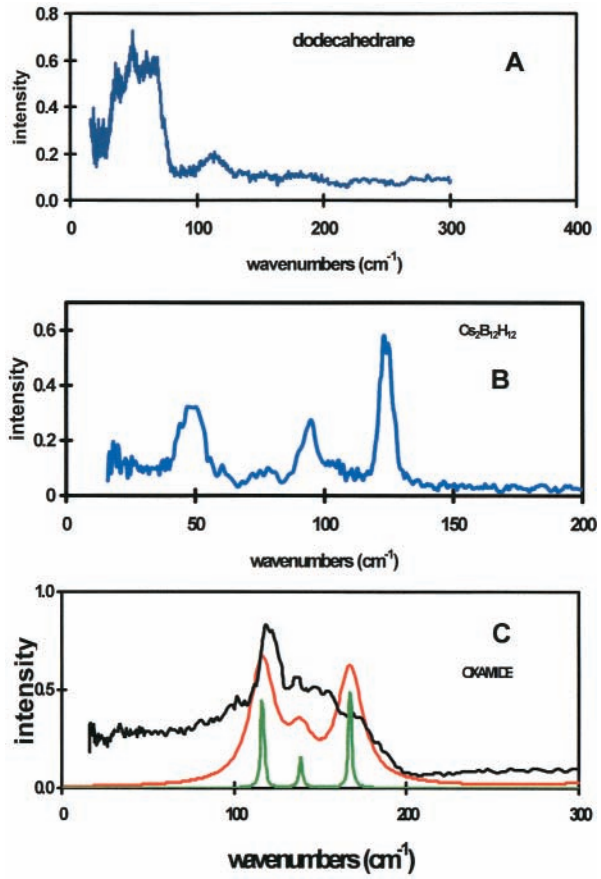

Figure 10. Low-frequency region of the spectra of three of the systems discussed in this paper showing the external or phonon features.

are produced as a pulse. These high-energy neutrons are moderated by collisions with (usually) hydrogen containing materials such as liquid hydrogen, liquid methane, or water. For the experiments described here, a hot water moderator is used. The distribution of neutrons that exits the moderator has a thermal distribution plus a residual tail of high energy neutrons that extends to several electronvolts. A similar facility, the first spallation source constructed, is the IPNS at Argonne National Laboratory.[28] Another is the Los Alamos Neutron Science Center (LANSCE).[29] ISIS is currently the brightest source of neutrons in the world. Plans are underway at ISIS to upgrade the proton current by approximately 50−60%. The USDOE Spallation Neutron Source (SNS)[30] is under construction near Oak Ridge National Laboratory. SNS is designed to be ca. 10 times brighter as a neutron source than the current ISIS brightness. A similar device is being considered for construction by the European Community.[31]

The spectrometer that we use at ISIS is called TOSCA.[32] This is a reincarnation of a machine called TFXA which has been extraordinarily productive.[33] These devices are time-of-flight crystal analyzer spectrometers. In this scheme, the transit time of a neutron from the moderator to the detector is determined. This is a known fixed distance. The final energy of the neutron is specified by a diffraction grating and a cold polycrystalline beryllium filter that serves as an order sorter. Because the final energy is specified, the transit time from sample to the detector is known, and thus, by subtraction from the total time, the transit time from the moderator to the sample is known. This specifies the initial energy. The sample temperature is ca. 10−20 K, so the neutron loses energy on collision. The final energy is specified to be 8 ± 3 cm^{-1}. With this arrangement, incident neutrons with an energy of 108 cm^{-1} (13.5 meV) will excite a vibration of 100 cm^{-1} and pass through the detector. Vibrational excitations of 1000 cm^{-1} utilize the neutron spectral component at 1008 cm^{-1}. Neutrons of this energy are called "epithermal". Spallation neutron sources are particularly useful in this energy region and higher. A monograph describes the design principles for pulsed neutron devices including this type of spectrometer.[34] A database of neutron spectra obtained with TFXA and TOSCA is available[35] as is a list of the over 400 publications that have resulted from use of these spectrometers.[33]

Thermal neutrons are also available from nuclear reactors. Since the recent closure of the HFBR Reactor at Brookhaven National Laboratories, the only available research reactor facilities in the US are HFIR at Oak Ridge,[36] NCNR at NIST,[37] and the research/teaching reactor at the University of Missouri.[38] The NIST site provides links to the many sites in Europe and throughout the world. The premier reactor based site in Europe is the Institute Laue Langevin in Grenoble, France.[39]

The NIST Center for Neutron research has recently (April 2000) initiated experiments using a new vibrational spectroscopy device called FANS (filter analyzer neutron spectrometer).[40] This device utilizes a monochromator to establish the incident neutron energy and a berylium filter cooled to 77K that, in combination with a graphite filter, specifies the final neutron energy to be below a cutoff of 1.1 meV. This also specifies the spectrometer resolution for low incident energies to be just under 10 cm^{-1}. For higher incident neutron energy, the monochromator and sample width result in an increase in the bandwidth to about 50 cm^{-1} at an energy exchange of 1000 cm^{-1}. The major advantage of the FANS design is that it permits a large number of detectors that subtend a large solid angle and thus very high neutron collection efficiency. This factor, in combination with a focusing monochromator providing a factor of 5 flux advantage, will permit reasonable quality spectra to be obtained for very small samples, perhaps as small as 10 mg for hydrogen containing materials. FANS currently has only half of its detector bank arrays installed and does not yet have the focusing monochromator. Spectra obtained with FANS in its present configuration are shown in Figures 8 and 9. In Figure 9, the spectrum of the pimelonitrile/urea complex obtained with FANS is compared with that obtained with TOSCA at ISIS when it was at 12 m ("TOSCA-1"). The new location of TOSCA at 17 m provides higher resolution at higher energy transfers.

Bibliography

There are several texts and monographs describing neutron scattering in general that include inelastic scattering and have small sections on vibrational inelastic scattering. The most accessible is that by Squires.[41] Perhaps the most authoritative general text is that by Lovesley.[42] There are several monographs that contain articles specific to molecular spectroscopy with neutrons including one edited by Egelstaff,[43] which contains an article by Janik and Kowalska that describes all of the equations given above and specifically the basic theory of scattering by harmonic oscillators developed by Zemach and Glauber.[44] There is also an elementary introduction to the entire field of neutron scattering, *Neutron Scattering: A Primer*, by Roger Pynn that is available at the LANCE web site.[29] Of greater relevance to chemists, there is a monograph edited by Willis, *Chemical Applications of Thermal Neutron Scattering*,[45] that includes an article by John White, one of the pioneers in this field, and another monograph by Boutin and Yip[46] that is entirely relevant to the subject of this review. Comparison of the spectra presented in either of these last two books with the spectra in

this review demonstrates how far the technique has advanced in the last 20−25 years. There are two recent review articles of relevance one by Mezei[47] on applications to materials science and an *Annual Reviews of Physical Chemistry* article.[48] Attention is called to the recent special issue of *Chemical Physics* on neutron scattering and modeling applications to condensed phase structure and dynamics[49] and also to an issue of *Spectrochemica Acta*[50] devoted to spectroscopic applications of INS. Finally, attention is called to the web site bibliography[51] of experiments performed with TFXA or TOSCA at ISIS.

Outlook

The combination of powerful new computational tools, the rapid growth of neutron facilities, and increased interest in condensed phase systems (including self-assembled systems and nanostructures) are leading to a new era in vibrational inelastic neutron scattering in particular and neutron science in general. These developments permit the inherent advantages of neutron scattering (sample penetration, isotopic specificity, interaction with nuclei not electrons, the variability of the length scale observed, and many others) to be much more fully utilized.

Acknowledgment. The Rutherford Appleton Laboratory is thanked for access to neutron beam facilities at the ISIS Facility. The NIST Center for Neutron Research is thanked for access to the FANS spectrometer at the NIST reactor facility. This work was partially supported by the US National Science Foundation under Grant CHE 9803058 and utilized the computer systems Exemplar and SGI PCarray at the National Center for Supercomputing Applications, University of Illinois at Urbana-Champaign. The author thanks Sergey Baronov, Dale Braden, Craig Brown, Tim Jenkins, Don Kearley, Julia Kuzmicheva, Chris Middleton, Dan Neumann, Stewart Parker, Horst Prinzbach, John Tomkinson, John Tse, Taner Yildirim, and Marek Zgierski for help in the course of this work.

References and Notes

(1) See http://www.ncnr.nist.gov/resources/n-lengths/ for data for other elements.

(2) Hudson, B. S.; Braden, D. A.; Parker, S. F.; Prinzbach, H. The vibrational inelastic neutron scattering spectrum of dodecahedrane: experiment and DFT simulation. *Angew. Chem., Int. Ed.* **2000**, *39*, 514−516 [*Angew. Chemie.* **2000**, *112*, 524−526].

(3) Tomkinson, J. (See http://www.isis.rl.ac.uk/molecularSpectroscopy/tosca/index.htm adamantane).

(4) Scott, A. P.; Radom, L. Harmonic Vibrational Frequencies−An Evaluation of Hartree−Fock, Moller−Plesset, Quadratic Configuration-Interaction, Density-Functional Theory, and Semiempirical Scale Factors. *J. Phys. Chem.* **1996**, *100*, 16502−16513.

(5) Hudson, B. S.; Parker, S. F. Unpublished results from TOSCA-1 at ISIS.

(6) Wunderlich, J.; Lipscomb, W. N. Structure of $B_{12}H_{12}$-2 Ion. *J. Am. Chem. Soc.* **1960**, *82*, 4427.

(7) Braden, D. A.; Hudson, B. S. C_6F_6 and sym-$C_6F_3H_3$: Ab initio and DFT Studies of Structure, Vibrations, and Inelastic Neutron Scattering Spectra. *J. Phys. Chem. A* **2000**, *104*, 982−989.

(8) Shimanouchi, T.; Mizushima, S.-I. *J. Chem. Phys.* **1949**, *17*, 1102.

(9) Parker, S. F.; Braden, D. A.; Tomkinson, J.; Hudson, B. S. Full Longitudinal Acoustic Mode (LAM) Spectrum of an *n*-Alkane: Comparison of Observed and Computed Incoherent Inelastic Neutron Scattering Spectrum of *n*-Octadecane. *J. Phys. Chem. B* **1998**, *102*, 5955−5956. Braden, D. A.; Parker, S. F.; Tomkinson, J.; Hudson, B. S. Inelastic Neutron Scattering Spectra of the Longitudinal Acoustic Modes of the Normal Alkanes from Pentane to Pentacosane. *J. Chem. Phys.* **1999**, *111*, 429−439.

(10) Parker, S. F.; Tomkinson, J.; Braden, D. A.; Hudson, B. S. Experimental test of the validity of the use of the *n*-alkanes as model compounds for polyethylene. *Chem. Commun.* **2000**, 165−166.

(11) Okada, K. Normal Frequencies of Skeletal Bending Vibration of Planar Zigzag Chain with Finite Length. *J. Chem. Phys.* **1965**, *43*, 2497.

(12) Hollingsworth, M. D.; Harris, K. D. M. *Compr. Supramol. Chem.* **1996**, *6*, 177; Atwood, J. L., Davies, J. E. D., MacNicol, D. D., Vogtle, F., Eds.

(13) Hudson, B. S. Oriented *n*-alkanes in urea-d_4 inclusion complexes for inelastic neutron scattering vibrational studies. *Mol. Cryst. Liq. Cryst.* **2001**, *356*, 423−432.

(14) Guo, H.; Karplus, M. Ab initio studies of hydrogen bonding on N_methylacetamide: structure, cooperativity, and internal rotational barriers. *J. Phys. Chem.* **1992**, *96*, 7273−7274.

(15) Tomkinson, J.; Kearley, G. J. Phonon wings in inelastic neutron scattering spectroscopy: The harmonic approximation. *J. Chem. Phys.* **1989**, *91*, 5164−5169.

(16) Kearley, G. J. A review of the analysis of molecular vibrations using INS. *Nucl. Instr. Methods Phys. Res. A* **1995**, *354*, 53−58.

(17) Hudson, B.; Tse, J.; Zgierski, M. Z.; Braden, D. A. The inelastic incoherent neutron spectrum of crystalline oxamide. *Chem. Phys.* **2000**, *261*, 249−260.

(18) Yildirim, T. Personal communication.

(19) Thomas, M. W.; Ghosh, R. E. Incoherent inelastic neutron scattering from hexamethylenetetramine and adamantane. *Mol. Phys.* **1975**, *29*, 1489−1506.

(20) Payne, M. C. Structure and Dynamics from First Principles. In *Proc. N2M Workshop on Neutrons and Numerical Methods, Grenoble, 1998*; AIP Press: Melville, NY, 1999; Vol. 479, Chapter 37, pp 3−8; Johnson, M. R., Kearley, G. J., Buttner, H. G., Eds. See also http://www.msi.com/materials/refs/castep/castep_topic.html.

(21) Delley, B. DMol3 DFT studies: from molecules and molecular environments to surfaces and solids. *Comput. Mater. Sci.* **2000**, *17*, 122−126. Delley, B. From molecules to solids with the Dmol3 approach. *J. Chem. Phys.* **2000**, *113*, 7756.

(22) Hudson, B.; Parker, S. F.; Yildirim, T.; Prinzbach, H. Manuscript in preparation.

(23) James, M. N. G.; Matsushima, M. Accurate Dimensions of the Maleate Monoanion in a Symmetric Environment not Dictated by Crystallographic Symmetry: Imidazolium Maleate. *Acta Crystallogr.* **1976**, *B32*, 1708−1713.

(24) Hollingsworth, M. D.; Brown, M. E.; Santarsiero, B. D.; Huffman, J. C.; Goss, C. R. Template-Directed Synthesis of 1:1 Layered Complexes of α,ω-Dinitriles and Urea: Packing Efficiency versus Specific Functional Group Interactions. *Chem. Mater.* **1994**, *6*, 1227−44.

(25) Etter, M. C.; Urbanczyk-Lipkowska, Z.; Jahn, D. A.; Frye, J. S. Solid-State Structural Characterization of 1,3-Cyclohexanedione and of a 6:1 Cyclohexanedione−Benzene Cyclamer Complex, a Novel Host−Guest Species. *J. Am. Chem. Soc.* **1986**, *108*, 5871−6.

(26) http://www.rl.ac.uk.

(27) http://www.isis.rl.ac.uk.

(28) http://www.pns.anl.gov.

(29) http://lansce.lanl.gov/.

(30) http://www.sns.gov.

(31) http://www.fz-juelich.de/ess/WIE/What_is_ess.html and http://www.fz-juelich.de/ess/HIS/ESS_History.html.

(32) http://www.isis.rl.ac.uk/molecularSpectroscopy/tosca/index.htm.

(33) http://www.isis.rl.ac.uk/molecularSpectroscopy/tosca/index.htm.

(34) Windsor, C. G. *Pulsed Neutron Scattering*; Halsted Press: New York, 1981.

(35) http://www.isis.rl.ac.uk/molecularSpectroscopy/tosca/index.htm.

(36) http://neutrons.ornl.gov/.

(37) http://www.ncnr.nist.gov/

(38) http://web.missouri.edu/~murrwww/.

(39) http://www.ill.fr/.

(40) http://webster.ncnr.nist.gov/instruments/fans.

(41) Squires, G. L. *Introduction to the Theory of Thermal Neutron Scattering*; Dover: Cambridge, 1978.

(42) Lovesey, S. W. *Theory of Neutron Scattering from Condensed Matter: Nuclear Scattering*; Clarendon Press: Oxford, 1984; Vols 1 and 2 (International Series of Monographs of Physics).

(43) Egelstaff, P. A. *Thermal Neutron Scattering*; Academic Press: New York, 1965.

(44) Zemach, A. C.; Glauber, R. J. *Phys. Rev.* **1954**, *94*, 118 and 169.

(45) Willis, B. T. M., *Chemical Applications of Thermal Neutron Scattering*; Oxford University Press: Oxford, 1973.

(46) Boutin, H.; Yip, S. *Molecular spectroscopy with neutrons*; M. I. T. Press: Cambridge, MA,1968.

(47) Mezei, F. Neutron Scattering: Application to Materials Science. *Diffus. Defect Data, Pt. B* **1997**, *56*, 133−144.

(48) Trouw, F. R.; Price, D. L. Chemical Applications of Neutron Scattering. *Annu. Rev. Phys. Chem.* **1999**, *50*, 571−601.

(49) Johnson, M. R., Kearley, G. J., Eckert, J., Eds. *Chem. Phys.* **2000**, *261*, 1−2.

(50) *Spectrochim. Acta*, **1992**, *48 A*, No. 3; Eckert, J., Kearley, G. J., Eds.

(51) http://www.isis.rl.ac.uk/molecularSpectroscopy/tosca.htm.